Supplementary Materials for

Decreased aviation leads to increased ice crystal number and a positive radiative effect in cirrus clouds

Jialei Zhu[1*], Joyce E. Penner[2*], Anne Garnier[3], Olivier Boucher[4], Meng Gao[5], Lei Song[6], Junjun Deng[1], Congqiang Liu[1], Pingqing Fu[1]

1 Institute of Surface-Earth System Science, School of Earth System Science, Tianjin University, Tianjin 300072, China

2 Department of Climate and Space Sciences and Engineering, University of Michigan, Ann Arbor, MI 48109, USA

3 Science Systems and Applications, Inc., Hampton, VA 23666, USA

4 Institut Pierre-Simon Laplace, Sorbonne Université / CNRS, Paris, France

5 Department of Geography, Hong Kong Baptist University, Hong Kong SAR, China

6 Center for Monsoon System Research, Institute of Atmospheric Physics, Chinese Academy of Sciences, Beijing 100029, China

Corresponding Author: Joyce E. Penner (penner@umich.edu) and Jialei Zhu (zhujialei@tju.edu.cn)

Key words: cirrus clouds, aircraft soot, COVID-19, radiative effects

This PDF file includes:

Figures S1 to S15

Tables S1 to S3

Text S1 to S2

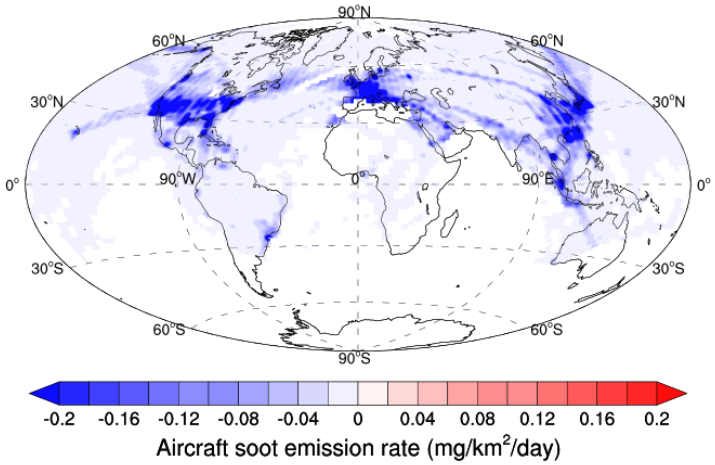

Figure S1. The difference in average aircraft soot emission rate in April/May between 2020 and 2019

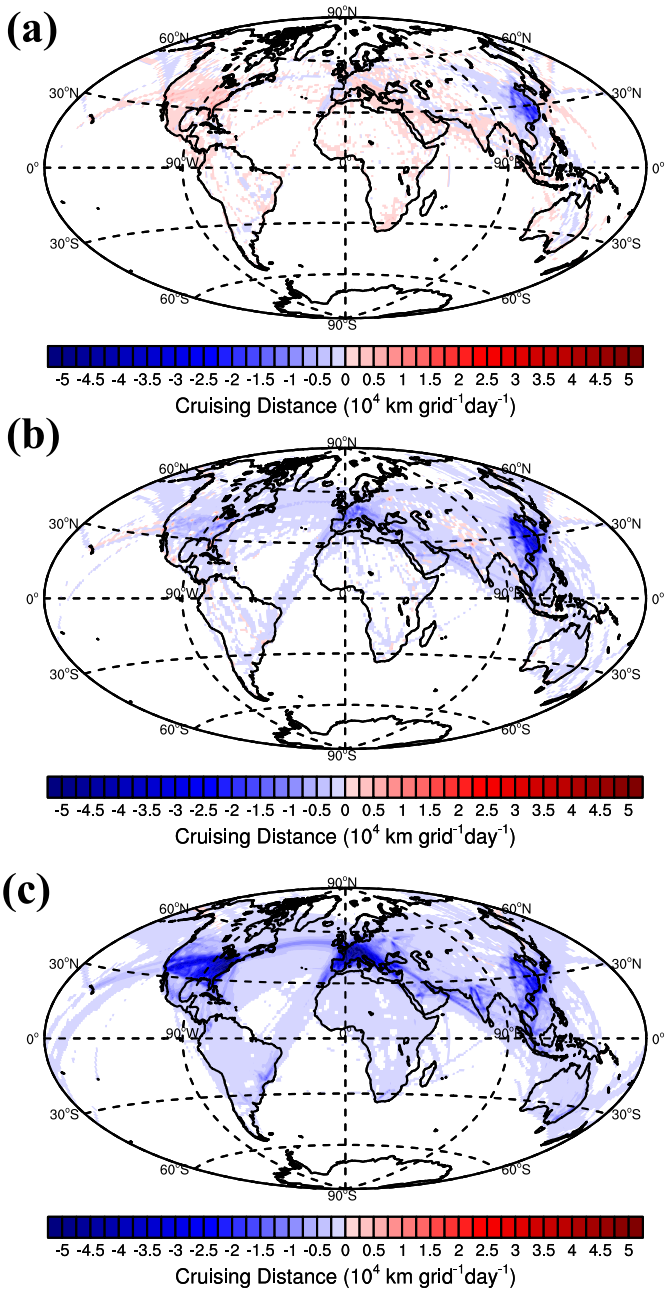

Figure S2. The difference in cruise distance (km grid^{-1} day^{-1}) between 2020 and 2019 in January/February (a), March (b) and April/May (c).

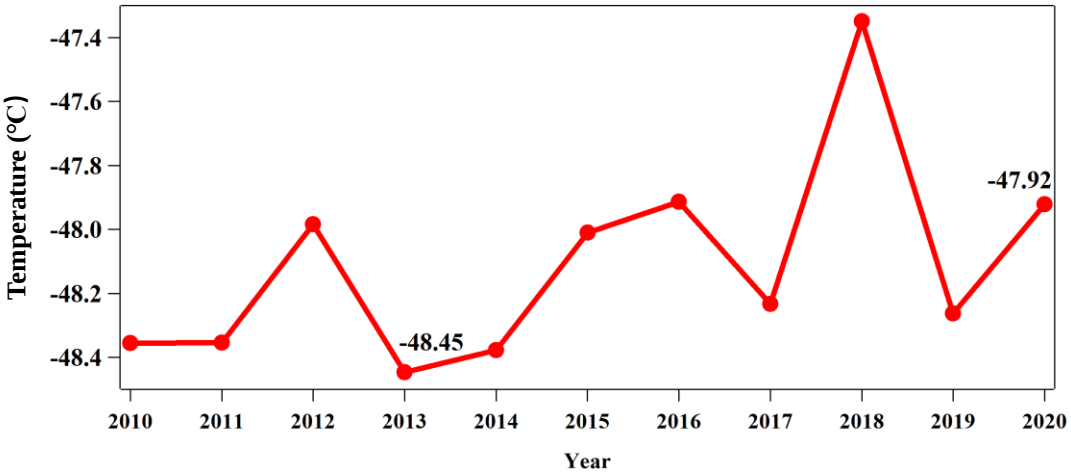

Figure S3. The average temperature in the 250-300hPa layer over 30°N-60°N in April/May based on NCEP reanalysis data.

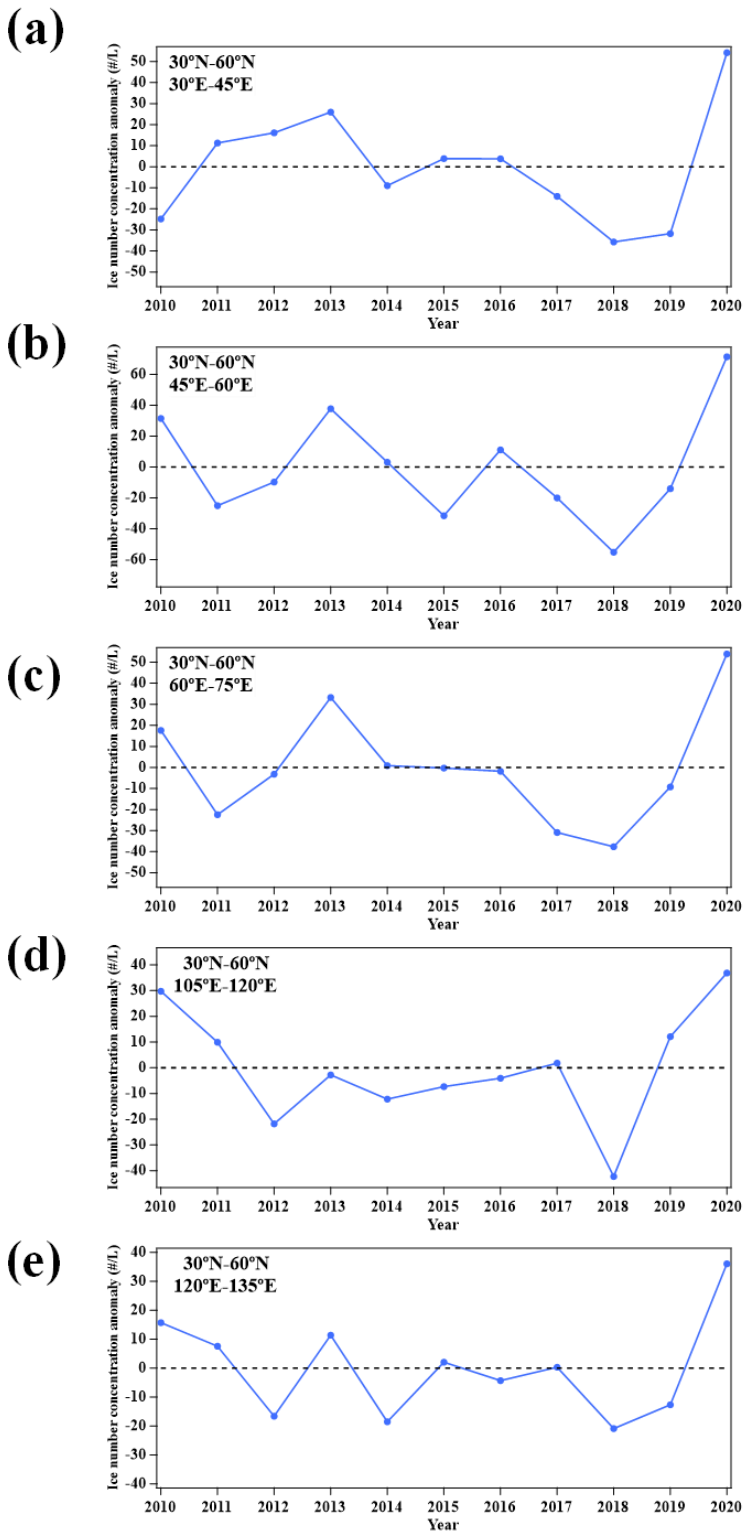

Figure S4. The median ice number concentration anomaly after detrending from 2010 to 2020 in the region of 30°E~45°E (a), 45°E~60°E (b), 60°E~75°E (c), 105°E~120°E (d), 120°E~135°E (e) in the latitude band from 30°N~60°N as observed by CALIPSO.

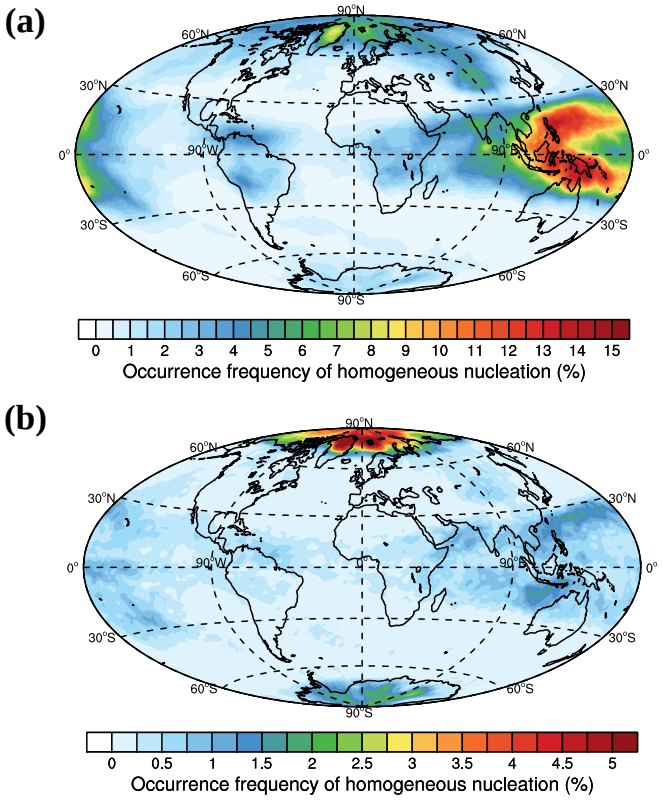

Figure S5. The simulated average occurrence frequency of homogeneous freezing (a) and that when constrained to CALIPSO observation conditions (ice water mixing ratios > 10^{-6} kg/kg and cloud optical depths between 0.3 and 3) (b) for January-May of 2018-2020.

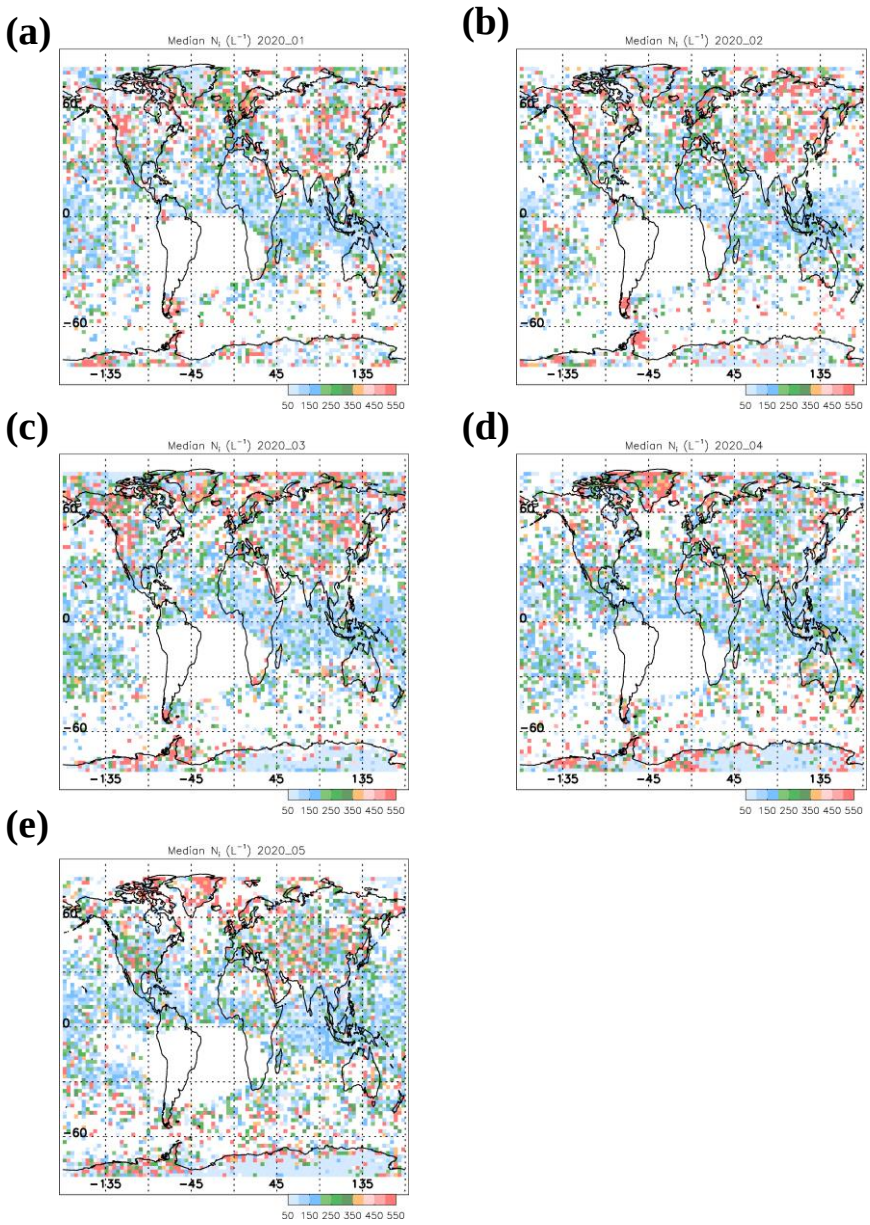

Figure S6. The median ice crystal number concentration (L^{-1}) in January (a), February (b), March (c), April (d) and May (e) of 2020 as observed by CALIPSO.

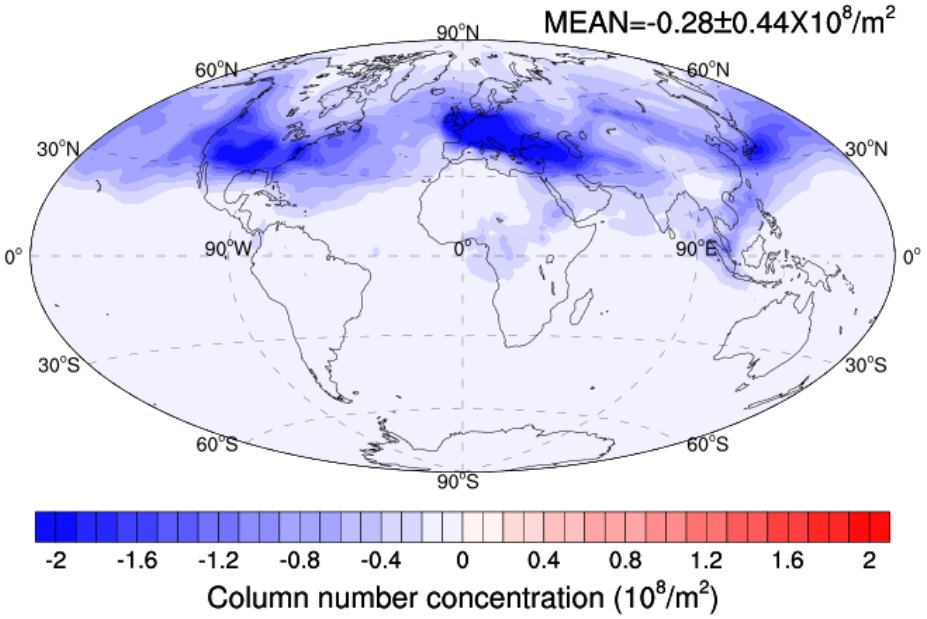

Figure S7. Reduction in the vertically integrated number concentration of contrail-processed aircraft soot (INPs) due to the COVID-19 pandemic in April-May 2020 compared to the assumption of no travel restriction (difference between EX_S2 and EX_S1).

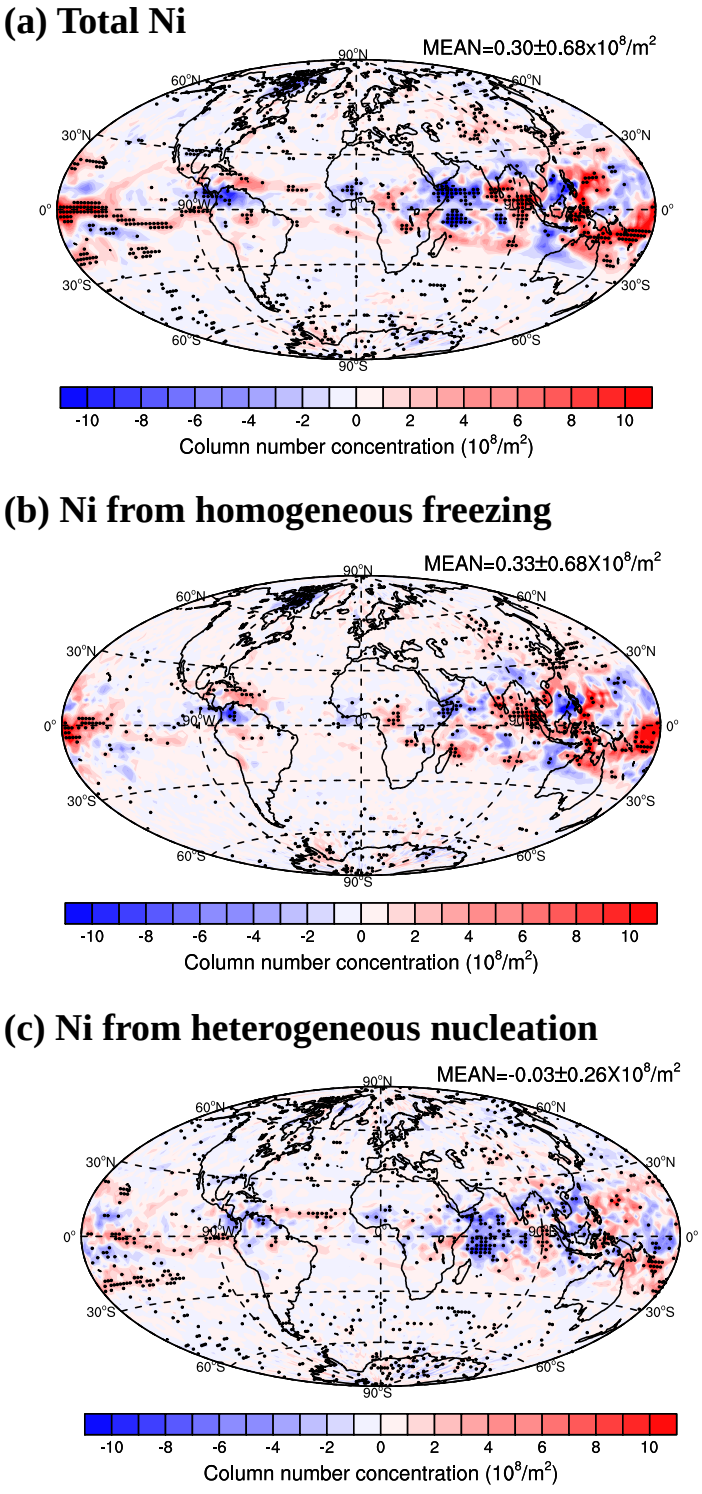

Figure S8. The change in the vertically integrated number concentration of grid-averaged total ice crystals (a), ice crystals from homogeneous freezing (b), and ice crystals from heterogeneous nucleation (c) due to the COVID-19 pandemic in April-May 2020 compared to the assumption of no travel restrictions (difference between EX_S2 and EX_S1). Differences significant at the 95% level according to a Student's t test are depicted by points.

(a) Ni from homogeneous freezing

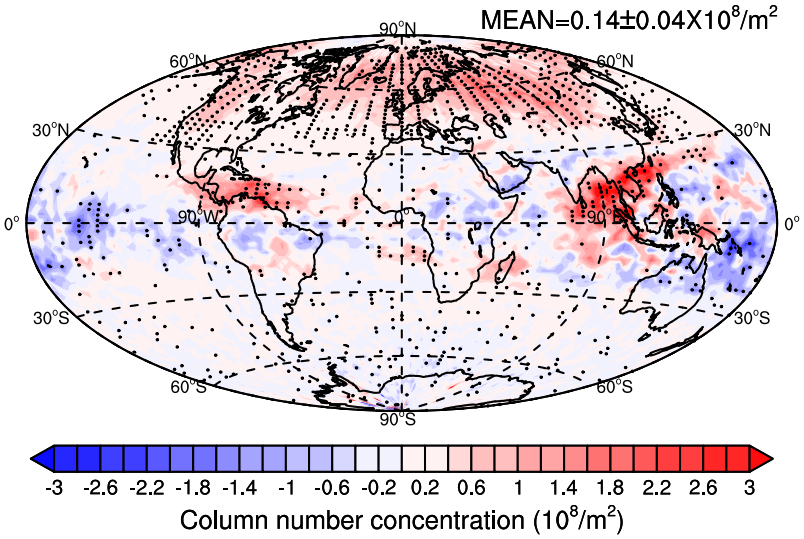

(b) Ni from heterogeneous nucleation

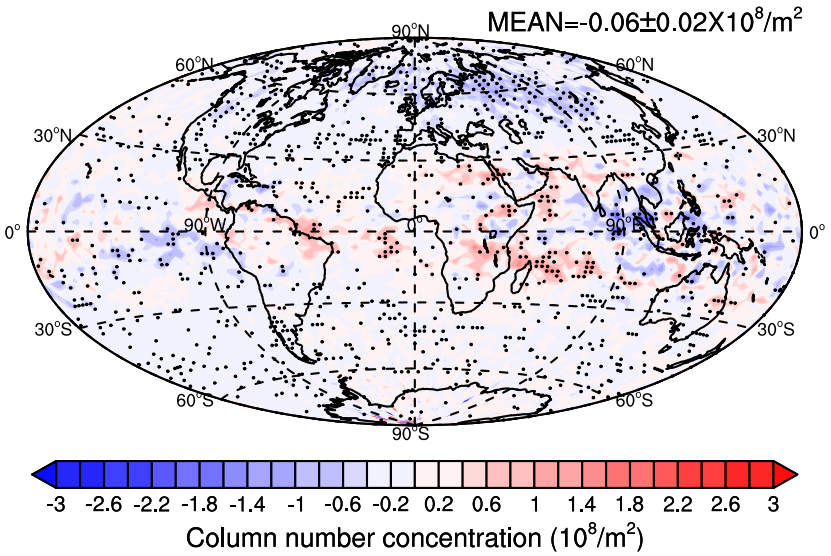

Figure S9. The change in the annual average vertically integrated grid-averaged number concentration of ice from homogeneous freezing (a) and ice from heterogeneous nucleation (b) due to a reduction in aircraft flights for five years (difference between cases EX_L2 and EX_L1). Differences significant at the 95% level according to a Student's t test are depicted by points.

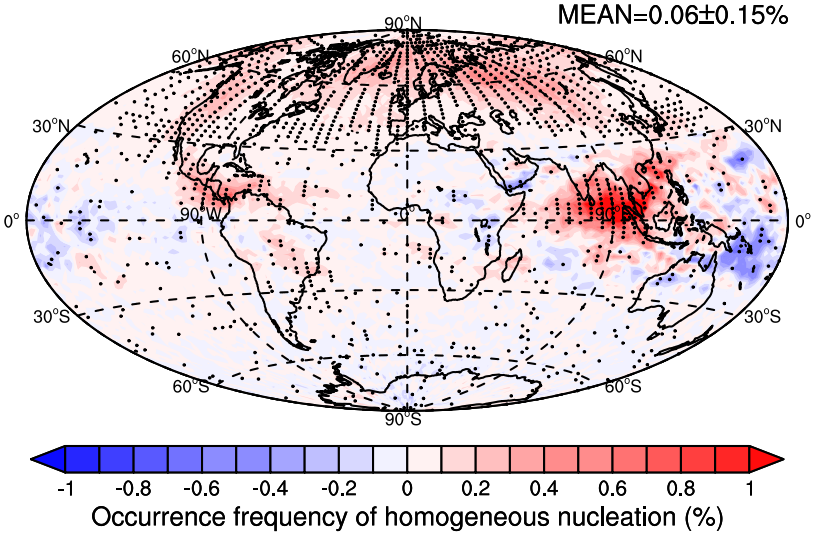

Figure S10. The change in the annual average occurrence frequency of homogeneous freezing due to a reduction in aircraft flights for five years (difference between cases EX_L2 and EX_L1). Differences significant at the 95% level according to a Student's t test are depicted by points.

(a) Longwave radiative effect

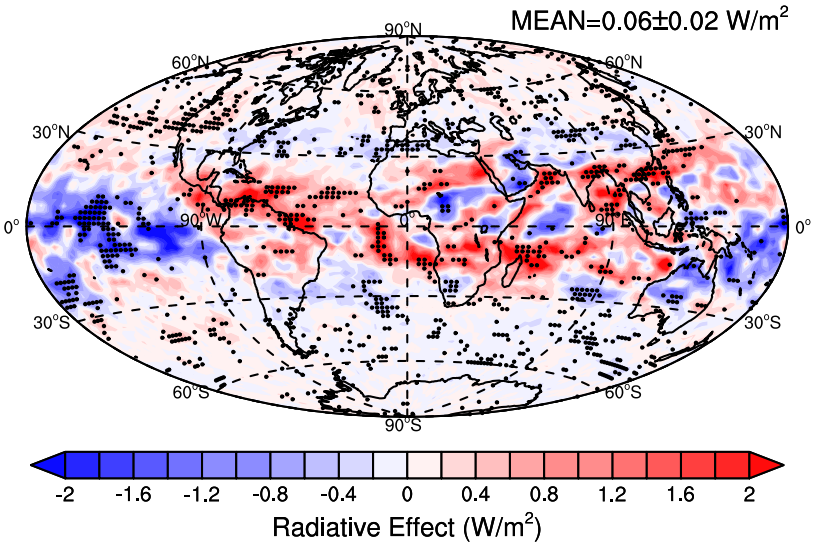

(b) Shortwave radiative effect

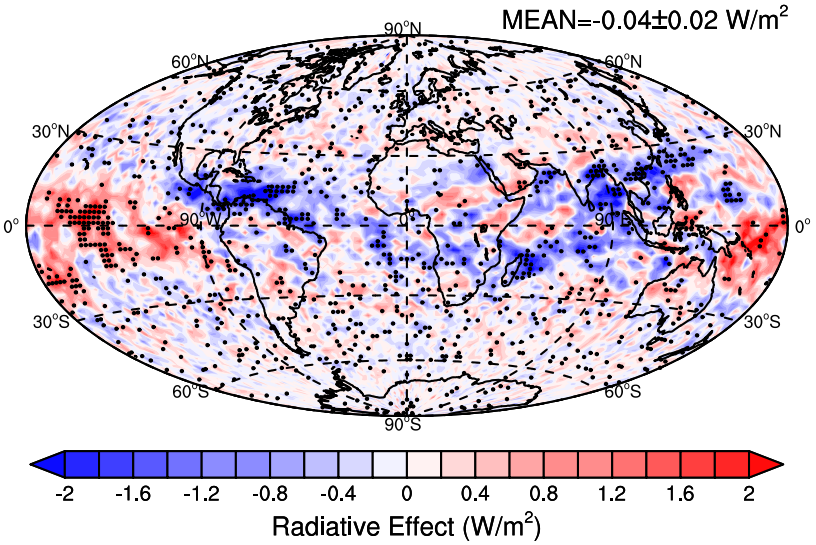

Figure S11. The change in the annual average all-sky longwave radiative effect (a) and all-sky shortwave radiative effect (b) due to a reduction of aircraft flights for five years (difference between cases EX_L2 and EX_L1). Differences significant at the 95% level according to a Student's t test are depicted by points.

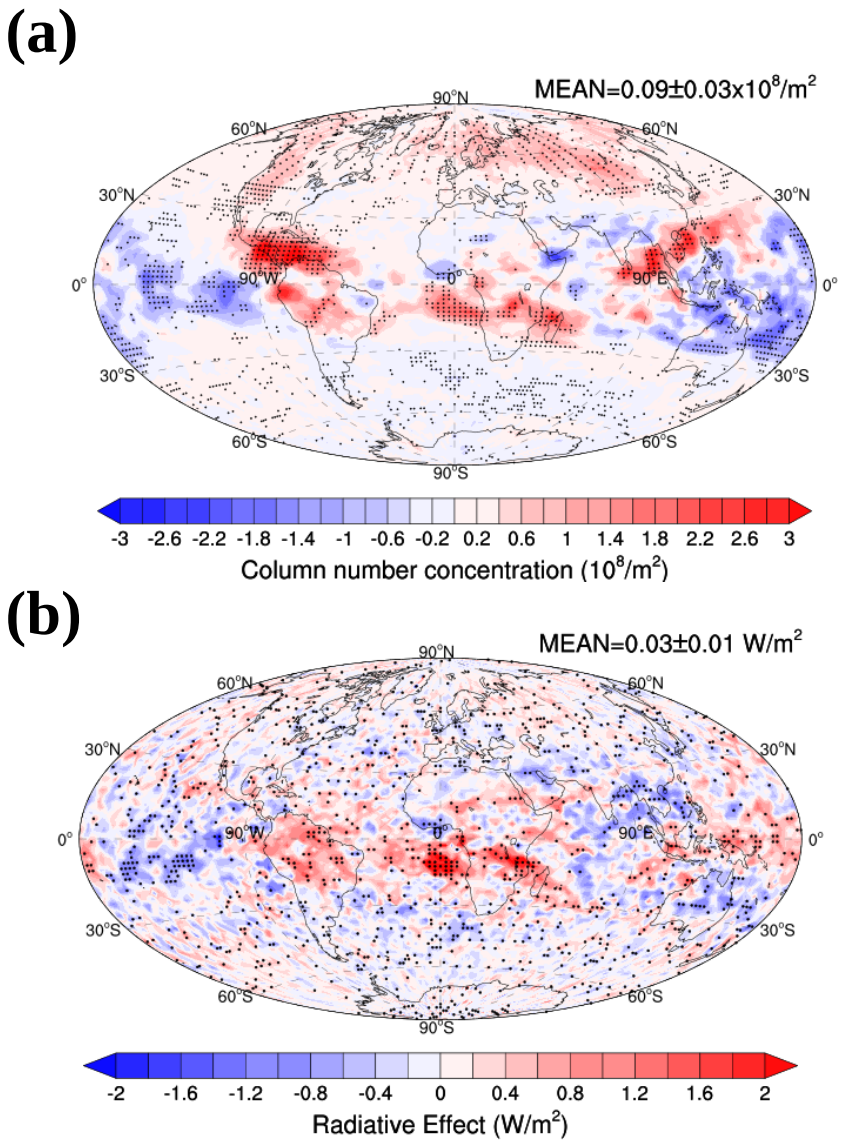

Figure S12. The change in the annual average vertically integrated number concentration (m^{-2}) of grid-averaged total ice crystals (a) and all-sky net radiative effect (W m^{-2}) (b) due to a flight decrease for five years in the sensitivity case excluding SOA as an efficient INP. Differences significant at the 95% level according to a Student's t test in (a) and (b) are depicted by points.

Table S1. Model-calculated difference in the median and average Ni (L^{-1}) between 2019 and 2018, 2020 and 2019, and 2020 and 2019 as well as the difference between 2020 and the average of 2019 and 2018.

			2019-2018	2020-2018	2020-2019	2020-AVE*
Jan-Feb	Median	60°S-60°N	11.78	***18.63***	6.85	10.14
		30°N-60°N	90.48	90.05	-0.43	44.81
		0°-30°N	-58.42	-10.2	48.21	19.01
		30°S-0°	***6.53***	-1.78	-8.31	-9.19
		60°S-30°S	8.53	-3.54	-12.08	-7.81
	Average	60°S-60°N	***33.94***	***34.15***	0.21	17.18
		30°N-60°N	***192.56***	***163.85***	-28.72	***67.57***
		0°-30°N	***-65.14***	-19.37	***45.77***	13.20
		30°S-0°	10.37	6.50	-3.86	1.32
		60°S-30°S	-2.04	-14.40	-12.35	-13.38
Apr-May	Median	60°S-60°N	***3.80***	7.01	3.21	5.62
		30°N-60°N	-0.50	18.34	18.84	18.59
		0°-30°N	3.35	17.9	14.55	16.23
		30°S-0°	-9.79	-9.06	0.73	-13.45
		60°S-30°S	22.16	0.87	-21.29	***-10.21***
	Average	60°S-60°N	14.27	***25.54***	11.26	***18.40***
		30°N-60°N	6.28	***56.07***	***49.79***	***52.93***
		0°-30°N	30.64	46.27	15.63	30.95
		30°S-0°	-14.7	-14.83	-0.13	-19.18
		60°S-30°S	34.88	14.64	-20.24	-2.80

Note: Italicized and bold numbers are statistically significant at the 95% level according to a Student's t test for the averages and a Mood's test for the medians.

*AVE stands for the average of Ni in 2018 and 2019.

Supplemental Text S1. The uncertainty in the effect of preexisting ice on ice nucleation

The effect of preexisting ice on ice nucleation has been discussed in previous studies (Zhou et al., 2016; Kuebbeler et al., 2014; Shi et al., 2015). Kärcher et al. (2006) recommended the use of their growth law for vapor deposition in the parameterization to describe deposition on preexisting ice particles. Kuebbeler et al. (2014) showed that preexisting ice can prevent high supersaturations and thereby prevent either homogeneous or heterogeneous freezing from occurring as a result of the effect of vapor deposition onto preexisting ice and can thereby reduce global ice crystal number and mass. Shi et al. (2015) found that the reduction of ice number concentration due to the effect of preexisting ice is significant at middle to high latitudes in the upper troposphere. Our previous study (Zhou et al., 2016) examined the ability and sensitivity of including a preexisting ice treatment to fit observed ice number concentrations and suggested excluding the treatment of preexisting ice in the parameterization. Our current model does not include consideration of the condensation of water vapor onto preexisting ice during the freezing of new particles. However, the inclusion or lack of preexisting ice during nucleation may lead to the uncertainties in the estimation of ice crystal number concentration. Considering the effect of preexisting ice correctly in the model is difficult. To our knowledge, there is still no global model treating the effect of preexisting ice well. As discussed in Penner et al. (2018), this choice of excluding the effect of preexisting ice is primarily dictated by the fact that within the CAM model, cloud fraction is determined by the grid box averaged RH and first updated at the new time step. Thus, it is impossible to distinguish if the cloud within a grid box is newly formed, had already existed at the previous time step, or is partially newly formed. If the ice cloud fraction or some of the cloud fraction was present during the previous time step, not including the rate of vapor deposition onto existing ice will overestimate ice number, since without deposition onto existing ice, the supersaturation predicted within model can be too large. So we used the grid box average RH to determine if ice forms

under cloud-free conditions.

Most models that include the treatment of preexisting ice assume that all new ice formation takes place within clouds, but use the grid average ice number concentration to determine the rate of deposition of water onto preexisting ice (Kuebbeler et al., 2014; Shi et al., 2015). This procedure is also incorrect, although, since the grid-average ice number is smaller than the in-cloud ice number, the use of this smaller ice number may somewhat account for the fact that some ice nucleation is expected within the ice-free portions of the grid. To determine the effect of preexisting ice on ice nucleation correctly, one would have to determine the newly formed cloud fraction within the ice-free portion of the grid and average this new ice with the ice number carried and/or newly formed in the existing cloud fraction from the previous time step.

As noted above, we used the expedient choice of using the grid box average RH to determine if ice forms under cloud-free conditions. If it does and this ice number is larger than the ice number in existing clouds, we replace it. We think that the new ice particles formed in the cloud-free portion of the grid would dominate the number formed in cloudy areas (because of the preexisting ice in cloudy areas), so this might be a better choice than assuming preexisting ice occurs across the entire grid, but with the grid-average number concentration as in other models, but more work is needed to establish this. We examined our predicted ice number concentration in comparison with observations as a method for calibrating any over-prediction in Penner et al. (2018) as well as in Zhu & Penner (2020).

Although we are still not able to include the effect of preexisting ice in the model correctly, we set up a sensitivity experiment (EX_S1) which assumed that no new ice nucleation took place in the cloudy portion of the sky that we had hoped would be an effective lower bound to the effect of preexisting ice on new ice formation. The average burden of ice crystal number concentration from Jan 2018 to May 2020 in EX_S1 was reduced by 97% compared to the case in the main text. As a result, the effect of the decrease in the aircraft soot emission during April/May 2020 on the integrated ice number is negligible for this sensitivity case (Figure S13), while it is 0.30×10^{8} m^{-2} for

the case in the main text (Figure S8a). However, for EX_S1, the median ice crystal number concentrations are underestimated by 65% in comparison to CALIPSO (Figure S14), while they are underestimated by only 21% using the method in the main text. Thus, we judge that this sensitivity test does not provide an effective lower bound. The treatment of preexisting ice in the global models and parameterizations still needs to be improved to better describe ice nucleation in the cloudy and clear sky portions of the grid.

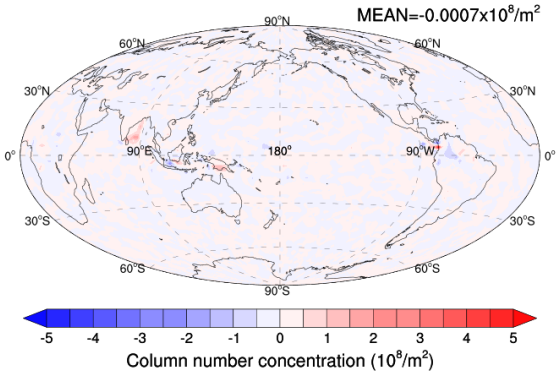

Figure S13. The change in the vertically integrated ice number concentration due to the COVID-19 pandemic in April-May 2020 with the assumption of no new ice nucleation in the cloudy portion of the sky (compare to Figure S8a)

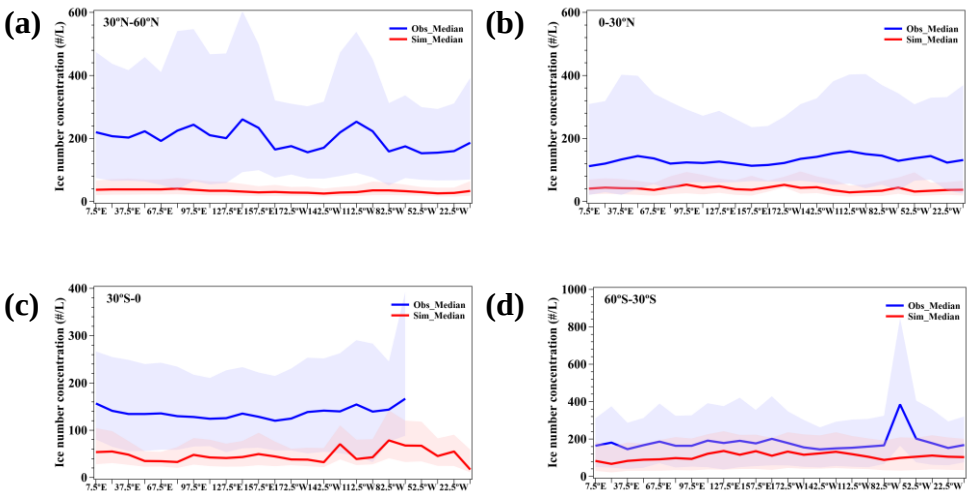

Figure S14. The comparison between CALIPSO observed (blue line) and simulated (red line) median ice number concentration (L^{-1}) in cirrus clouds for 30°N~60°N (a), 0~30°N (b), 30°S~0 (c), and 60°S~30°S (d) during January-May from 2018 to 2020 for the sensitivity case EX_S1. The shading represents the 25th and 75th percentiles of the median (compare to Figure 2 in main text).

We also note that aircraft contrails are known to increase cloud fraction in regions of frequent flights. This could also lead to an increase in ice crystal number concentration as a result of the removal of cloud fraction due to the decrease in aircraft flights. We examined the importance of this possible explanation for the CALIPSO overservations by comparing the MODIS satellite observations of high cloud fraction for April/May 2020 with that from previous years. Table S2 shows the change in high cloud fraction (over regions similar to those in Table 1 in the paper):

Table S2. The difference in the high cloud fraction retrieved from MODIS for different years

	2019-2018	2020-2018	2020-2019	2020-AVE1	2020-AVE2
60°S-60°N	0.0013	-0.0010	-0.0023	-0.0017	-0.0030
30°N-60°N	0.0090	-0.0031	-0.0121	-0.0076	-0.0074
0°-30°N	-0.0200	-0.0092	0.0108	0.0008	-0.0012
30°S-0°	0.0129	0.0023	-0.0106	-0.0042	-0.0069
60°S-30°S	0.0046	0.0072	0.0026	0.0049	0.0043

AVE1 is the average of 2018-2019
AVE2 is the average of 2010-2019

While most of these differences are negative, indicating that the removal of aircraft contrails in 2020 may have decreased cloud fraction, none are significant at a 90% significance level. Table S3 shows a similar calculation using the modeled changes in cloud fraction:

Table S3. The simulated difference in the high cloud fraction

	2019-2018	2020-2018	2020-2019	2020-AVE1
60°S-60°N	-0.0141	-0.0323	-0.0182	-0.0252
30°N-60°N	0.0426	0.0181	-0.0245	-0.0032
0°-30°N	-0.0049	-0.0003	0.0046	0.0022
30°S-0°	-0.0890	-0.1420	-0.0530	-0.0975
60°S-30°S	-0.0052	-0.0050	0.0002	-0.0024

AVE1 is the average of 2018-2019

An advanced analysis of the effects of natural cloud feedback as a result of contrail formation, shows that natural clouds decrease when contrails form (so if contrails are

removed, natural cloud would increase) (Bickel et al., 2020). As shown in that paper, while this feedback is not sufficient to completely offset the radiative forcing by contrails, it is substantial, and thus, this mechanism may explain the small cloud fraction changes seen in the MODIS data and model results above. Thus, it seems that while a decrease in cloud fraction as an explanation for the increase in Ni observed by CALIPSO may be partly responsible, it may be less important than changes in Ni resulting from the decrease in aircraft soot.

Supplemental Text S2. The potential influence of coating of aircraft soot on ice nucleation

The coating on aircraft soot by sulfate and secondary organic aerosols could change its ability to act as INP. Our model was developed so that if there is a coating by sulfate of > 3 monolayers on aircraft soot, the soot no longer acts as an INP. This treatment follows the same treatment we use for the coating of dust by sulfate which is consistent with the results of field studies by DeMott et al. (2003), Cziczo et al. (2004), and Richardson et al. (2007) (see discussion in Penner et al. (2018)). In addition to coating by sulfate, the model simulates coating by secondary organic aerosol (SOA) on aircraft soot, although there is no change in the ability of the soot to act as an INP as a result of SOA coating, in part because SOA can become glassy and act as an INP in any case. We examined the differences in the coatings of aircraft soot in April/May between 2020 and the average of 2018/2019 to examine the potential influence of these coatings on ice nucleation during the COVID-19 pandemic lockdown. We found that both the global average burden of the sulfuric acid and SOA coatings on aircraft soot were decreased in April/May 2020 compared to the same months in 2018/2019, because the coating is preferentially deposited on other aerosols as the result of decrease in the aircraft soot, although the burden of coatings increased at high latitudes of the Southern Hemisphere (Figure S15a, c). Moreover, the ratio of the coating burdens to aircraft soot burden was calculated. The ratio of sulfuric acid coating to aircraft soot was increased in most regions in April/May 2020 compared to 2018/2019, except for some regions in western Asia and Europe where the sulfuric coating burden decreased (Figure S15b). The ratio of SOA coating to aircraft soot was increased in the Northern Hemisphere and most tropical regions (Figure S15d).

Nevertheless, we are unable to quantify the effect of these coatings on cirrus cloud formation because the influence of these coatings on the ability of aircraft soot to act as an INP remains uncertain and cannot be parameterized. Mahrt et al. (2020) indicated that propane soots aged in sulfuric acid solutions enhanced ice nucleation activity compared to the fresh soot, but Möhler et al. (2005) found that the coating of soot from

a sparc-discharge generator with sulfuric acid decreased ice nucleation. The Mahrt et al. (2020) study did not specify the amount of sulfuric acid on the soot, but if the Mahrt et al. (2020) result holds, the increased ratio of sulfuric acid coating to aircraft soot shown in the model may result in an increase in ice nucleation (in contrast to our treatment which decreases ice nucleation for > 3 monolayers of sulfuric acid coating, based on observations of dust). Zhang et al. (2020) found that SOA coating on BC could either have almost no effect on its ice nucleating capability or inhibit ice nucleation, depending on the source and type of SOA. The strength of the decrease in IN activity with different types of SOA was suggested to be due to a change in phase state overcoming the effect of IN inhibition (i.e. becoming more amorphous). Thus, it remains unknown as to whether the increased SOA coating on aircraft soot in the model in April/May 2020 would lead to a reduction of ice nucleation. The net effect of the combined sulfuric acid and SOA coating on aircraft soot was not estimated based on these limited experimental results.

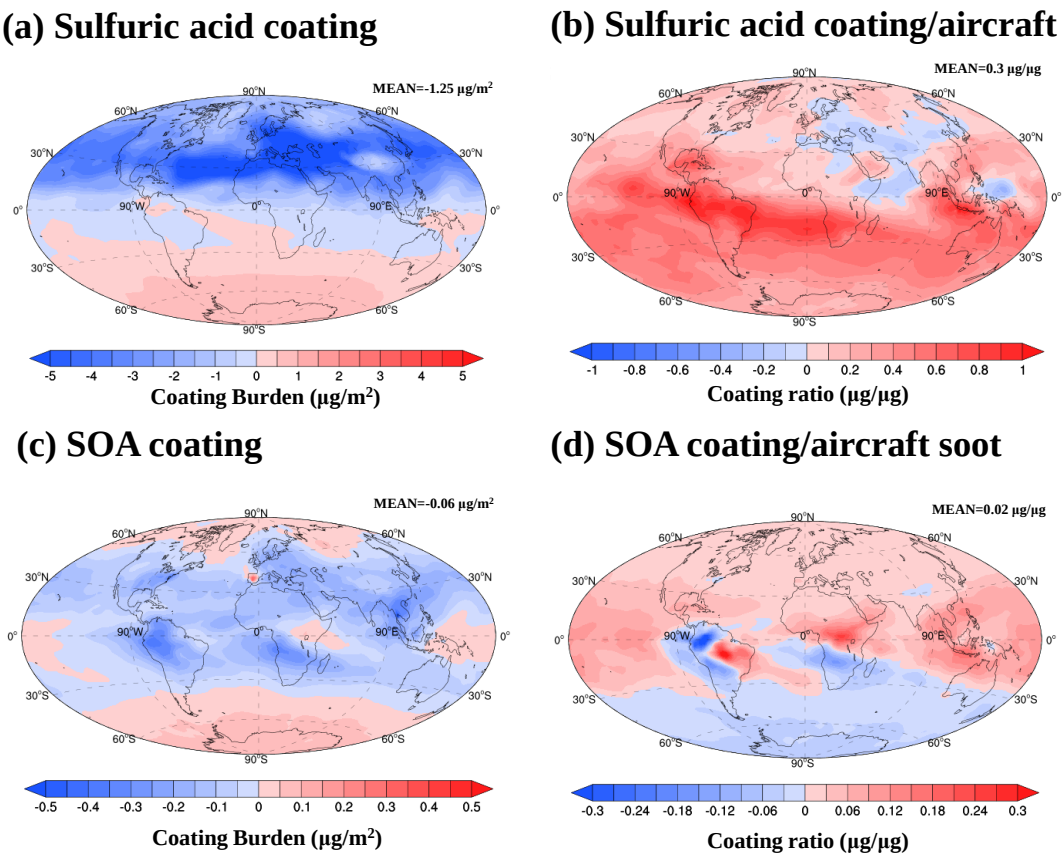

Figure S15. The difference in the burden of sulfuric acid coating (a) and SOA coating (c) on aircraft soot, as well as the ratio of sulfuric acid coating (b) and SOA coating (d) to aircraft soot in April/May between 2020 and the average of 2018/2019.

References

Cziczo, D. J., Murphy, D. M., Hudson, P. K., & Thomson, D. S. (2004). Single particle measurements of the chemical composition of cirrus ice residue during CRYSTAL-FACE. Journal of Geophysical Research, 109, D04201. https://doi.org/10.1029/2003JD004032

DeMott, P. J., Sassen, K., Poellot, M. R., Baumgardner, D., Rogers, D. C., Brooks, S. D., et al. (2003). African dust aerosols as atmospheric ice nuclei. Geophysical Research Letters, 30(14), 1732. https://doi.org/10.1029/2003GL017410

Kärcher, B., Hendricks, J., & Lohmann, U. (2006). Physically based parameterization of cirrus cloud formation for use in global atmospheric models. *Journal of Geophysical Research, 111*(D1).

Kuebbeler, M., Lohmann, U., Hendricks, J., & Kärcher, B. (2014). Dust ice nuclei effects on cirrus clouds. *Atmos. Chem. Phys., 14*(6), 3027-3046. https://acp.copernicus.org/articles/14/3027/2014/

Mahrt, F., Alpert, P. A., Dou, J., Gronquist, P., Arroyo, P. C., Ammann, M., et al. (2020). Aging induced changes in ice nucleation activity of combustion aerosol as determined by near edge X-ray absorption fine structure (NEXAFS) spectroscopy. Environ Sci Process Impacts, 22(4), 895-907. https://www.ncbi.nlm.nih.gov/pubmed/32188960

Mohler, O., et al. (2005), Effect of sulfuric acid coating on heterogeneous ice nucleation by soot aerosol particles, Journal of Geophysical Research-Atmospheres, 110(D11), doi:10.1029/2004jd005169.

Penner, J. E., Zhou, C., Garnier, A., & Mitchell, D. L. (2018). Anthropogenic Aerosol Indirect Effects in Cirrus Clouds. *Journal of Geophysical Research: Atmospheres, 123*(20), 11,652-611,677.

Richardson, M. S., DeMott, P. J., Kreidenweis, S. M., Cziczo, D. J., Dunlea, E. J., Jimenez, J. L., et al. (2007). Measurements of heterogeneous ice nuclei in the western United States in springtime and their relation to aerosol characteristics. Journal of Geophysical Research, 112, D02209. https://doi.org/10.1029/2006JD007500

Shi, X., Liu, X., & Zhang, K. (2015). Effects of pre-existing ice crystals on cirrus clouds and comparison between different ice nucleation parameterizations with the Community Atmosphere Model (CAM5). *Atmospheric Chemistry and Physics, 15*(3), 1503-1520.

Zhou, C., Penner, J. E., Lin, G., Liu, X., & Wang, M. (2016). What controls the low ice number concentration in the upper troposphere? *Atmospheric Chemistry and Physics, 16*(19), 12411-12424.

Zhang, C., Y. Zhang, M. J. Wolf, L. Nichman, C. Shen, T. B. Onasch, L. Chen, and D. J. Cziczo (2020), The effects of morphology, mobility size, and secondary organic aerosol (SOA) material coating on the ice nucleation activity of black carbon in the cirrus regime, Atmospheric Chemistry and Physics, 20(22), 13957-13984, doi:10.5194/acp-20-13957-2020.

Zhu, J., & Penner, J. E. (2020). Radiative forcing of anthropogenic aerosols on cirrus clouds using a hybrid ice nucleation scheme. *Atmospheric Chemistry and Physics, 20*(13), 7801-7827.